

Enzymes

Direct Observation of Kinetic Pathways of Biomolecular Recognition

Susobhan Choudhury,^[a] Subrata Batabyal,^[a] Prasanna Kumar Mondal,^[a] Priya Singh,^[a] Peter Lemmens,^{*[b]} and Samir Kumar Pal^{*[a]}

Abstract: The pathways of molecular recognition, which is a central event in all biological processes, belong to the most important subjects of contemporary research in biomolecular science. By using fluorescence spectroscopy in a microfluidics channel, it can be determined that molecular recognition of α -chymotrypsin in hydrous surroundings at two different pH values (3.6 and 6.3) follows two distinctly different pathways. Whereas one corroborates an induced-fit model (pH 3.6), the other one (pH 6.3) is consistent with the selected-fit model of biomolecular recognition. The role of

massive structural perturbations of differential recognition pathways could be ruled out by earlier XRD studies, rather was consistent with the femtosecond-resolved observation of dynamic flexibility of the protein at different pH values. At low concentrations of ligands, the selected-fit model dominates, whereas increasing the ligand concentration leads to the induced-fit model. From molecular modelling and experimental results, the timescale associated with the conformational flexibility of the protein plays a key role in the selection of a pathway in biomolecular recognition.

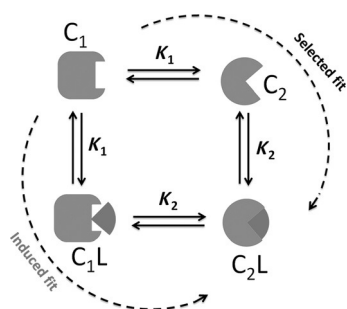
Introduction

In all biological processes, biomolecular recognition related to small ligands is a central phenomenon. For the past 50 years, ligand-induced conformations and changes to biological macromolecules (induced-fit) proposed by Koshland have been textbook explanations for recognition events.^[1] However, recent theoretical and experimental studies suggest an alternative pathway in which small ligands select and stabilise a complementary, lowest energy conformation from a pre-existing equilibrium of ground and excited states of the bio-molecules (selected fit).^[2–6] In all of these cases, the binding interaction does not induce conformational changes. Importantly, over the past decade, high-resolution NMR relaxation, single-molecule spectroscopy, Förster resonance energy transfer (FRET) analysis and molecular dynamic simulations have shone more light on the conformational diversity of proteins in solution.^[7–17] In recent reports, the key factor for the characteristic difference between on and off rates in the two mechanisms is concluded to be conformation and relaxation of the bio-molecules. Whether a protein binds to its ligand through a selected-fit or

induced-fit mechanism can be identified by perturbing the conformational equilibrium (Scheme 1). Several experimental strategies have been suggested to demonstrate recognition pathways, including mutation,^[18–22] which perturbs the conformational equilibrium of the involved protein. However, concise experimental demonstrations of these two pathways are sparse in the literature. This is the motivation for our present work. Furthermore, we aim to investigate biochemical strategies that involve specific mutations far from the protein-binding pockets without altering the recognition site.^[23] Such mutations may alter the step-wise conformation changes required for competent binding.^[24] The calculation of conformational free energy differences in the unbound and bound states is well established, but requires experimental protein structures in both the unbound and ligand-bound states, which is challenging in most cases.^[6] An alternative experimental strategy has been employed here that involves perturbation of the host solvent to control conformational relaxation of the proteins under study. The X-ray crystal structure of the α -chymotrypsin^[25] (CHT) monomer has been studied and found to be unchanged at both pH values (3.6 and 6.3) investigated.^[26] However, the mobility of water molecules at the surface of the protein is observed to change with pH. The hydration shell of biological macromolecules plays a crucial role on their stability and in the recognition of a specific site.^[27] Femtosecond dynamic studies have provided insights into more ordered water molecules on the overall surface of the above-mentioned protein at low pH values.^[28] The rigid water structure at low pH (3.6) inhibits the dynamics and functionality of proteins, whereas a mobile and less rigid hydration surface at high pH (6.3) makes the active recognition dynamically favourable. For enzymatic activity, the dynamics of the active site is essential, how-

[a] S. Choudhury, Dr. S. Batabyal, Dr. P. K. Mondal, P. Singh, Prof. S. K. Pal
Department of Chemical, Biological and Macromolecular Sciences
S. N. Bose National Centre for Basic Sciences
Block JD, Sector III, Salt Lake, Kolkata 700 098 (India)
E-mail: skpal@bose.res.in

[b] Prof. P. Lemmens
Institute for Condensed Matter Physics and Laboratory for Emergent
Nanometrology, TU Braunschweig, Mendelssohnstrasse 3
38106 Braunschweig (Germany)
E-mail: p.Lemmens@tu-bs.de



Scheme 1. Schematic representation of the simple four-state model of protein–ligand binding. C_1 and C_2 are the two conformations of the protein and L is the binding ligand. K_1 and K_2 are the corresponding binding constants.^[6]

ever, the function and dynamics of the probe site (opposite to the active site in the present case) are correlated.

In most biochemical reactions, such as protein folding, protein–ligand interactions occur rapidly, and thus, need to be triggered on very short timescales to study their kinetics.^[25,29,30] In this direction, we have studied molecular recognition (of biological systems/biomimetic) and enzyme kinetics in a microfluidics system equipped with a microscopic and spectroscopic attachment.^[31] Herein, we used 8-anilino-1-naphthalenesulfonic acid ammonium salt (ANS) and CHT as a model ligand and protein, respectively. The enhancement of fluorescence intensity as a manifestation of the complexation of ANS with CHT is followed along the microfluidics channel. The kinetic profile of the fluorescence enhancement of ANS with CHT at pH 3.6 and 6.3 along the microchannel shows two distinct pathways. Theoretical fitting of the kinetic data in the two pH values reveals different pathways of molecular recognition of ANS by the protein CHT. In a control experiment, we studied the interaction between a non-biological cetrimonium bromide (CTAB) micelle with ANS under similar experimental conditions to rule out the role of the host solvent for the observed differential recognition pathways of CHT. We show herein that the binding mechanism shifts towards induced-fit from selected-fit upon increasing the ligand concentration. We also performed simulations by using the COMSOL Multiphysics program to interpret our experimental data.

Results and Discussion

A simple four-state model^[32–34] of CHT–ANS binding in the microfluidics channel is shown in Figure 1. An H-shaped microfluidics channel with two inlets, one for the enzyme CHT (120 μM) in buffer at a specific pH value and another for ANS (10 μM) in the buffer solution, was used to generate the time gradient of the CHT–ANS complex along the direction of flow in the channel. The flow rates through each of the two inlets were held constant at 50 $\mu\text{L min}^{-1}$, which corresponded to an average linear (laminar) flow of 100 $\mu\text{L min}^{-1}$ in the main channel. This value of average laminar flow was obtained from the volumetric flow rate of the fluid and cross-sectional area of the microchannel. The estimated time resolution in the experimental conditions along the microchannel is 18.85 $\mu\text{s } \mu\text{m}^{-1}$.

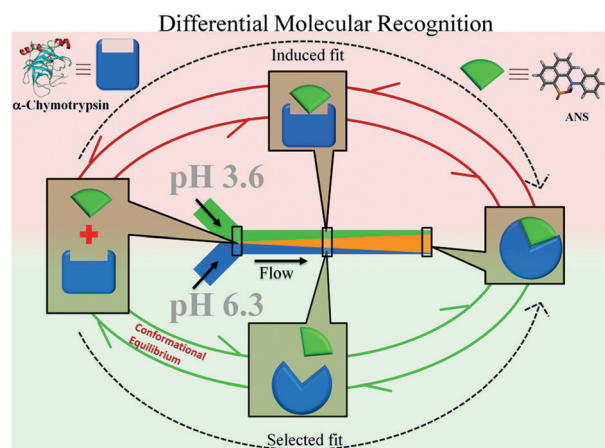


Figure 1. Schematic representation of the H-shaped microfluidics channel used for molecular recognition studies at different pH values in a four-state model. The difference between these two pathways is that at higher pH (6.3) the ligand (ANS) interacts with the pre-existing ensemble of protein conformations through a selected-fit mechanism, whereas at low pH (3.6) the bound protein conformation forms only after interaction with the ligand (see text).

The fluorescence micrographs of the microfluidics channel corresponding to the two different experimental conditions are shown in Figure 2a. The blue–green emission from the ANS–CHT complex increases along the channel because ANS and CHT have time to be mixed to form the ANS–CHT complex. The intensity of the emission from the ANS–CHT complex is much higher at pH 3.6. The inset of Figure 2b shows the fluorescence spectra of the ANS–CHT complex with different pH buffers. The enhancement of the fluorescence quantum yield at pH 3.6 is clearly evident and is consistent with earlier studies.^[28,35] The evolution of fluorescence enhancement as a function of time along the microchannel shows two distinct pathways (Figure 2b).

To explain our experimental kinetics data, we considered a simple kinetics scheme of $A \rightarrow B \rightarrow C$, with the corresponding first-order rate constants of k_1 and k_2 for the formation of the intermediate (B) from the substrate (A) to the final product (C), in which substrate A represents the unbound (without ANS) form of the enzyme CHT; B is the intermediate state of CHT with ANS, immediately after recognition; and C is the final form of the CHT–ANS complex. Herein, we have considered two important approximations: firstly, k_1 is the rate of formation of the CHT–ANS complex; thus, should it be of second order. However, because the concentration of the enzyme CHT in our case is much higher than that of ANS (at least 10 times to rule out the emission of ANS itself in solvent), k_1 can be approximated as a pseudo-first-order rate constant. Secondly, the back reaction rates are taken to be slow enough to consider two consecutive reactions to be irreversible, which is in agreement with a steady-state approximation in the system. The assumption of an almost irreversible binding of the ligand ANS with the protein CHT is supported by the earlier experimental observation that the ligand is strongly bound to the protein over the 3.6–7.0 pH range, which reveals an amalgamated protein–ligand complex.^[35] A unique binding site of ANS to the

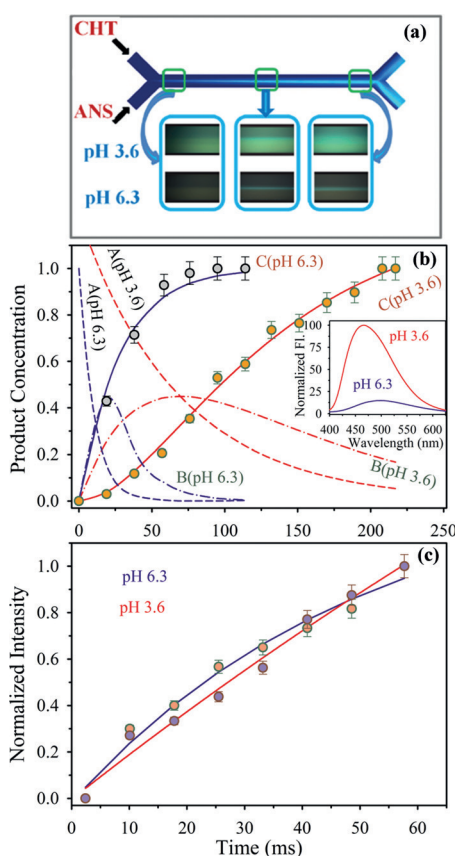


Figure 2. The fluorescence and kinetics results are compared at two pH values. a) Micrographs of the microfluidics channel at different positions along the channel at different pH values. b) Evolution of the emission intensity of ANS upon complexation with CHT along the microfluidics channel (solid lines). The substrate (A) and intermediate (B) concentrations at different pH values are shown with dotted lines. Steady-state fluorescence spectra of ANS with CHT at different pH values are shown in the inset. c) Molecular recognition pathways of a cationic CTAB micelle at different pH values in the microfluidics channel (see text).

protein in the pH range has been explored in an X-ray crystallographic study.^[26] Considering the above conditions, one may write the time evolution of [C] as Equation (1):^[36]

$$[C] = a \left(1 + \frac{k_1 e^{-k_2 t} - k_2 e^{-k_1 t}}{k_2 - k_1} \right) \quad (1)$$

and the concentrations of the substrate (A) and intermediate (B) can be written as Equations (2) and (3):

$$[A] = a e^{-k_1 t} \quad (2)$$

$$[B] = \frac{a k_1}{k_2 - k_1} (e^{-k_1 t} - e^{-k_2 t}) \quad (3)$$

in which a denotes the initial concentration of CHT at time $t = 0$. Numerical fitting of the experimental data with Equation (1) reveals a reasonable agreement with the analytical model of

the intermediate-state formation. In the case of pH 6.3, the k_1 and k_2 values were found to be 1000 and 36.7 s^{-1} , respectively. On the other hand, at pH 3.6, the numerical values of k_1 and k_2 were 14.2 and 14.5 s^{-1} , respectively. The above analytical and approximated solutions should now be compared to decide whether the steady-state approximation is valid in the context of two pathways of molecular recognition of CHT at pH 6.3 and 3.6. In the former case (pH 6.3), first A transforms into B rapidly and B accumulates because it disappears slowly. As the concentration of A decreases, its rate of transformation decreases; at the same time the rate of conversion of B into C increases as more B is formed, so a maximum is reached when Equation (4) is satisfied:

$$t = \frac{\ln(k_1/k_2)}{k_1 - k_2} \quad (4)$$

As long as $k_1 \neq k_2$, the concentration of B decreases as shown in Figure 2b. The observation is consistent with the fact that a pre-selected conformation of the enzyme CHT makes complexation with the ligand ANS “fast” and only then undergoes a structural reorganisation, leading to the recognition pathway on the selected-fit mechanism.^[6,37] From the magnitude of the obtained pseudo-first-order reaction rate to its corresponding second-order rate constant, we derive a value of $10^7 \text{ M}^{-1} \text{ s}^{-1}$, which is consistent with that of the reported value.^[38] The first-order rate constant, k_2 , for structural reorganisation of the enzyme is also of the same order as the reported value^[38] of $10\text{--}100 \text{ s}^{-1}$. In the latter case (pH 3.6), when the enzyme is less flexible and biologically inactive,^[26,28] the pseudo-first-order rate constant, k_1 , is much slower than that of the former case. The estimated second-order rate constant is about $1.4 \times 10^5 \text{ M}^{-1} \text{ s}^{-1}$, which is in agreement with weak binding of ANS to CHT in the first stage.^[38] Afterwards, structural reorganisation follows a similar time constant; however, it is smaller in magnitude than in the former case. The molecular recognition pathway involving much weaker binding in the first stage and complexation through structural reorganisation is consistent with the induced-fit mechanism.

Experimental artefacts due to the dimerisation of the probe ligand at lower pH^[39] in the observation of the differential pathways of molecular recognition can be ruled out for the following reasons: Careful experiments^[39] show that the ligand remains in its monomeric form at about $\approx 100 \mu\text{M}$ at pH 3, 5 and 7. The concentration used in our experiment is around $10 \mu\text{M}$. Moreover, in a control experiment on the complexation of ANS (anionic) with cationic CTAB micelles (inset of Figure 2c) under similar experimental conditions, we obtained k_1 and k_2 values of 1486 and 19.8 s^{-1} , respectively, for pH 6.3, whereas at pH 3.6 the corresponding k_1 and k_2 values were 1076 and 10.0 s^{-1} , respectively. This observation clearly rules out the possibility of any interference of the host buffer (of different pH) with the differential CHT–ANS complexation kinetics at the two pH values discussed above. Conversion of the pseudo-first-order rate constant, k_1 , to its second-order counterpart reveals a value of $10^4 \text{ M}^{-1} \text{ s}^{-1}$, which is consistent with the reported value of molecular complexation of an organic

ligand with a micelle.^[40] The observed similarity of the kinetic pathway in the case of the CTAB micelle at two different pH values is in agreement with recognition through a selected-fit mechanism, in which the spherically symmetric micelles are always ready (in the pre-selected conformation) to recognise the ligand ANS at first with a minor structural adjustment (k_2) following thereafter. The first-order rate constants k_2 ($\approx 10 \text{ s}^{-1}$) are also in agreement with the structural relaxation timescale of a micelle reported in the literature.^[41]

Various studies^[42,43] have suggested that the protein–ligand binding mechanism can be shifted from selected- to induced-fit upon increasing the ligand concentration because in the presence of a higher ligand concentration complexation becomes more favourable, assuming an enhanced probability of complexation before the conformational transition of the protein. However, this cannot be fully confirmed without additional information on protein–ligand interactions and dynamic studies of the protein. Using a molecular dynamics simulation of a model protein–ligand system, Greives and Zhou have shown that both the rate of the conformational transition and the concentration of ligand molecules can affect the induced-fit fraction.^[44] The effect of ligand concentration on the shifting binding mechanism can be easily understood from our experiments. The fluorescence micrographs of the microfluidics channel with different ligand concentrations are shown in Figure 3a. It is evident from the results shown in Figure 3b that the selected-fit mechanism at pH 6.3 is shifted towards the induced-fit mechanism with increasing ligand concentration at a fixed protein concentration.

The numerical fitting of experimental data at various ligand concentrations with Equation (1) reveals reasonable agreement with the fact that the increasing ligand concentration leads to changes from selected- to induced-fit behaviour. The fitting parameters are tabulated in Table 1 within experimental error ($\pm 8\%$). The protein conformations convert into the active one in the absence of any ligand molecule and then continue in the active conformation until a ligand molecule completes the binding reaction by complexation. At a low ligand concentration, the protein is free from any ligand molecules most of the time; thus the selected-fit mechanism dominates. At high ligand concentrations, conformational changes occur followed by binding processes because most of the time the ligand molecule will be inside the binding pocket, and thus, the binding mechanism will shift toward the induced-fit mechanism.^[44]

The experimentally observed differential molecular recognition pathways were simulated by using COMSOL Multiphysics (v4.3a) software by coupling the physics of laminar flow and reaction kinetics (Figure 4). A 3D geometry was created based on the dimensions of the microchannel used in our experiment with two inlets and two outlets (H channel). To consider species diffusion, the convection and diffusion model (transport of diluted species) was included in the fluid flow physics. The diffusion constants of CHT and ANS used were 0.5×10^{-10} and $1 \times 10^{-10} \text{ m}^2 \text{ s}^{-1}$, respectively, as reported previously.^[45,46] The simulation was carried out with a flow of ANS through the lower inlet and CHT in the upper inlet. The simulation yielded a concentration profile of enzymes in the presence of a substrate

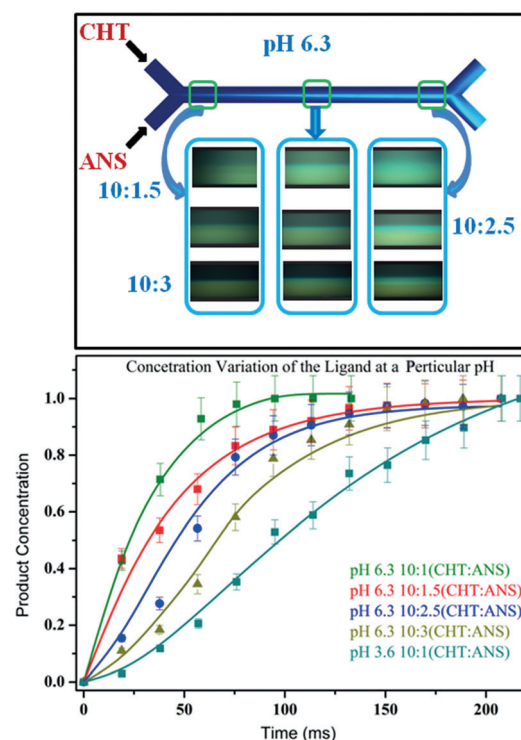


Figure 3. Effect of ligand concentration on the binding mechanism. a) Micrographs of the microfluidics channel at different positions along the channel with different concentrations of ligand at pH 6.3. b) Comparison of normalised emission intensity of ANS upon binding CHT along the microfluidics channel at different concentration of ANS at pH 6.3 and 3.6.

Table 1. Numerically fitted kinetic parameters.

Concentration ratio (CHT/ANS)	k_1 [s^{-1}]	k_2 [s^{-1}]
10:1 (pH 6.3)	1000	36.7
10:1.5 (pH 6.3)	715.1	23.3
10:2.5 (pH 6.3)	179.5	19.9
10:3 (pH 6.3)	62.7	17.1
10:1 (pH 3.6)	14.2	14.5

gradient.^[47] Figure 4 represents the inter-diffusional zone of the two interacting species along the channel at different times related to the spatial distribution of the interacting species at several positions in the reaction zone. For representation purposes, the initial, middle and final sections of the channel, where the simulation has been executed are shown. The inter-diffusion zone is critically governed by the molecular diffusivity of the individual species. Figure 4 represents a comparative observation of the rate if the fluorescence intensity changes due to the molecular recognition kinetics with diffusion limited by molecular interactions. Figure 4a depicts a comparison of experimental data at pH 3.6 with simulated data obtained from the induced-fit model. The contour plots representing the concentration of CHT–ANS complex at several positions along the channel and colour bars representing the normalised concentration are also shown in Figure 4. We also compared the experimental data at pH 6.3 with molecular simulation data by using the selected-fit model (Figure 4b).

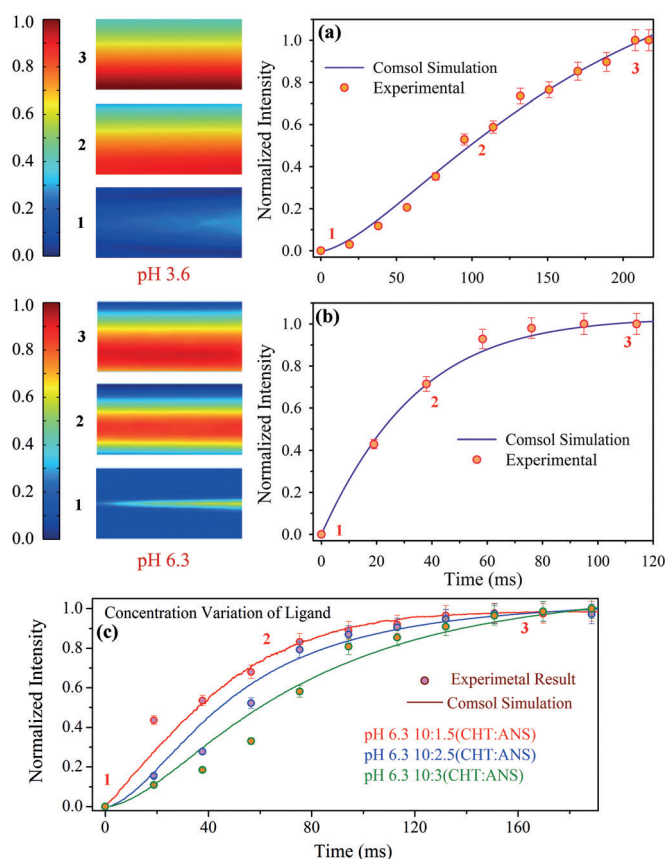


Figure 4. Simulated results compared with experimental results. The simulated concentration gradient of the CHT–ANS complex at different pH values is shown in the left panel. The right panel shows the agreement of the simulation results (solid line) with that of the experimental data (scattered points) at different pH values. The shifting of the binding mechanism is shown with increasing ligand concentration at pH 6.3. Here, 1–3 represent contour plots of the complex formation at three different positions in the microfluidics channel.

By comparing the experimental results with the simulated results, one can see that the interaction of ANS with CHT at different pH values follows different mechanisms. Our simulation results show that the interaction of the CHT enzyme with the ANS substrate follows the selected-fit mechanism at pH 6.3 to yield k_1 and k_2 values of 1000 and 29.9 s^{-1} . On the other hand, at pH 3.6, k_1 and k_2 have values of 14.42 and 14.44 s^{-1} , respectively. A simulation of CHT with different concentrations of ANS substrate at pH 6.3 (Figure 4c) yielded k_1 and k_2 values that were consistent with our experimental results (Table 2). With increasing ligand concentration, a shifting of the binding mechanism can be observed by the sigmoidal shapes of the experimental data at pH 6.3. The simulated results also show sigmoidal shapes at higher concentrations of the ligand, although there are some deviations from experimental results that are within the experimental error limit ($\pm 5\%$). Therefore, the simulated results are in reasonably good agreement with our experimental results, which suggests that the overall interaction of the ligand with the model biomimetic system can be described by simple reaction models. The molecular recognition of CHT with ANS is not simply diffusion limited, but rather follows different mechanisms at different pH values.

Table 2. Kinetic parameters obtained from simulations with the COMSOL Multiphysics program.

Concentration ratio (CHT/ANS)	k_1 [s^{-1}]	k_2 [s^{-1}]
10:1 (pH 6.3)	1000	29.9
10:1.5 (pH 6.3)	715.6	23.5
10:2.5 (pH 6.3)	165.5	20.3
10:3 (pH 6.3)	59.1	16.8
10:1 (pH 3.6)	14.2	14.4

Conclusion

We demonstrated two different pathways of molecular recognition, namely, selected- (conformational selection) and induced-fit mechanisms, of CHT by a small organic ligand, ANS, in a microfluidics channel at two different pH values. Whereas the structural flexibility of the protein at pH 6.3 triggered selected-fit, restricted protein motion at pH 3.6 prompted the protein to adopt induced-fit molecular recognition. We also showed that at pH 6.3 increasing ligand concentration led to a change in the binding mechanism from selected- to induced-fit at a fixed protein concentration. We correlated our experimental data with a simple analytical model and simulation that relied on the steady-state approximation for the generation of a product through intermediate species. Our findings might have an immediate and positive impact on efforts to design and engineer proteins with new functions.

Experimental Section

Chemicals

ANS was purchased from Sigma–Aldrich. CTAB was purchased from Fluka chemicals. CHT was purchased from Sigma–Aldrich. The materials were of the highest commercially available grades and were used without further purification.

Experimental details

Steady-state fluorescence measurements were carried out by using a Jobin–Yvon Fluoromax-3 fluorimeter. Microfluidics experiments were carried out with an H-shaped microchannel (Dolomite, UK) coupled to a fluorescence microscope (Olympus BX51, Olympus America, Inc.). The two inlets of the microchannel were attached to a syringe pump by capillary tubes. The capillaries were passed through the shaft of the holder prior to connection with the microfluidic chip. The reagents were propelled by using a syringe pump (Atlas-ASP011, Syrris Ltd.) and the total volumetric flow rate was adjusted according to requirements. Fluorescence images were captured with a fluorescence microscope equipped with a 100 W mercury arc lamp, which was used as the excitation source (UV-light excitation) and a TUCSEN TCH-5.0ICE camera. The excitation light was cut off by using a standard filter and the fluorescence was collected through a $10\times$ objective. Image processing and analyses were achieved by using the ANALYSIS software provided with the microscope. A region of interest^[29] (ROI) was selected at a specific height and width. This ROI was used to obtain an intensity profile along the microchannel. Intensity profiles were acquired at a particular microchannel distance from the initial mixing confluence. The RGB analysis was performed and the individual colour in-

tensity was monitored with time. Fluorescence intensity values were normalised to a maximum value of one. This channel distance was converted into the reaction time by dividing it by the velocity of the flow. The observed fluorescence intensities were fitted with the commercially available software SCIENTIST by creating a new model that followed the equation for the rate of formation of different components.

COMSOL simulation

The fluid dynamics simulation was carried out by using the COMSOL multiphysics software (v4.3a) with a finite element method. A 3D geometry was created based on the dimensions (length 12.5 mm, radius 100 μm) of the microchannel used in our experiment with two inlets and two outlets (H channel). Herein, we used two models for two pH values. For pH 3.6, we chose the model $A + C \rightarrow B \rightarrow P$, in which A, C, B, and P were ANS, CHT, intermediate complexes of the ANS–CHT, and the final ANS–CHT product. For high pH (6.3), the model was different leading to $C \rightarrow C^* \xrightarrow{A} P$, in which C^* was another conformation of CHT. To simulate the fluid flow in the microchannel, a model of laminar flow was added to the simulation. By considering diffusion of the species, the convection and diffusion model (transport of diluted species) was coupled to the fluid flow physics. The rate of product formation in the system equalled the rate of substrate depletion. Concentration profiles generated in COMSOL were exported as text files.

Acknowledgements

S.C. and S.B. thank the CSIR, India, for the research fellowships. We thank DST (India) for financial grants (SB/S1/PC-011/2013 and DST/TM/SERI/2k11/103) and DAE (India) for grant 2013/37P/73/BRNS. P.L. thanks the NTH-School "Contacts in Nanosystems: Interactions, Control and Quantum Dynamics", the Braunschweig International Graduate School of Metrology, and DFG-RTG 1952/1, Metrology for Complex Nanosystems.

Keywords: bioinformatics · enzymes · kinetics · molecular modeling · molecular recognition

- [1] D. Koshland, Jr., *Proc. Natl. Acad. Sci. USA* **1958**, *44*, 98–104.
- [2] C.-J. Tsai, S. Kumar, B. Ma, R. Nussinov, *Protein Sci.* **1999**, *8*, 1181–1190.
- [3] C. J. Tsai, B. Ma, Y. Y. Sham, S. Kumar, R. Nussinov, *Proteins: Struct. Funct. Genet.* **2001**, *44*, 418–427.
- [4] K. A. Dill, H. S. Chan, *Nat. Struct. Biol.* **1997**, *4*, 10–19.
- [5] J. D. Bryngelson, J. N. Onuchic, N. D. Socci, P. G. Wolynes, *Proteins: Struct. Funct. Genet.* **1995**, *21*, 167–195.
- [6] T. R. Weikl, C. von Deuster, *Proteins Struct. Funct. Bioinf.* **2009**, *75*, 104–110.
- [7] C. Tang, C. D. Schwieters, G. M. Clore, *Nature* **2007**, *449*, 1078–1082.
- [8] Z.-L. Lu, M. Coetsee, C. D. White, R. P. Millar, *J. Biol. Chem.* **2007**, *282*, 17921–17929.
- [9] A. Mittermaier, L. E. Kay, *Science* **2006**, *312*, 224–228.
- [10] H. Frauenfelder, S. G. Sligar, P. G. Wolynes, *Science* **1991**, *254*, 1598–1603.
- [11] P. K. Agarwal, S. R. Billeter, P. R. Rajagopalan, S. J. Benkovic, S. Hammes-Schiffer, *Proc. Natl. Acad. Sci. USA* **2002**, *99*, 2794–2799.

- [12] K. Henzler-Wildman, D. Kern, *Nature* **2007**, *450*, 964–972.
- [13] D. D. Boehr, H. J. Dyson, P. E. Wright, *Chem. Rev.* **2006**, *106*, 3055–3079.
- [14] A. C. M. Ferreon, J. C. Ferreon, P. E. Wright, A. A. Deniz, *Nature* **2013**, *498*, 390–394.
- [15] L. J. Lapidus, S. Acharya, C. R. Schwantes, L. Wu, D. Shukla, M. King, S. J. DeCamp and V. S. Pande, *Biophys. J.* **2014**, *107*, 947–955.
- [16] M. Gruebele, *J. Am. Chem. Soc.* **2014**, *136*, 16695–16697.
- [17] S. Choudhury, P. K. Mondal, V. K. Sharma, S. Mitra, V. G. Sakai, R. Mukhopadhyay, S. K. Pal, *J. Phys. Chem. B* **2015**, *119*, 10849–10857.
- [18] C. E. Cameron, S. J. Benkovic, *Biochemistry* **1997**, *36*, 15792–15800.
- [19] G. P. Miller, S. J. Benkovic, *Biochemistry* **1998**, *37*, 6327–6335.
- [20] L. Wang, N. M. Goodey, S. J. Benkovic, A. Kohen, *Proc. Natl. Acad. Sci. USA* **2006**, *103*, 15753–15758.
- [21] A. D. Vogt, E. Di Cera, *Biochemistry* **2013**, *52*, 5723–5729.
- [22] A. D. Vogt, E. Di Cera, *Biochemistry* **2012**, *51*, 5894–5902.
- [23] P. A. Romero, F. H. Arnold, *Nat. Rev. Mol. Cell Biol.* **2009**, *10*, 866–876.
- [24] S. Kumar, B. Ma, C. J. Tsai, N. Sinha, R. Nussinov, *Protein Sci.* **2000**, *9*, 10–19.
- [25] W. A. Eaton, V. Muñoz, S. J. Hagen, G. S. Jas, L. J. Lapidus, E. R. Henry, J. Hofrichter, *Annu. Rev. Biophys. Biomol. Struct.* **2000**, *29*, 327–359.
- [26] L. D. Weber, A. Tulinsky, J. D. Johnson, M. A. El-Bayoumi, *Biochemistry* **1979**, *18*, 1297–1303.
- [27] P. Ball, *Chem. Rev.* **2008**, *108*, 74–108.
- [28] S. K. Pal, J. Peon, A. H. Zewail, *Proc. Natl. Acad. Sci. USA* **2002**, *99*, 15297–15302.
- [29] Y. Gambin, C. Simonnet, V. VanDelinder, A. Deniz, A. Groisman, *Lab Chip* **2010**, *10*, 598–609.
- [30] S. J. DeCamp, A. N. Naganathan, S. A. Waldauer, O. Bakajin, L. J. Lapidus, *Biophys. J.* **2009**, *97*, 1772–1777.
- [31] S. Batabyal, S. Rakshit, S. Kar, S. K. Pal, *Rev. Sci. Instrum.* **2012**, *83*, 043113–043119.
- [32] S. M. Sullivan, T. Holyoak, *Proc. Natl. Acad. Sci. USA* **2008**, *105*, 13829–13834.
- [33] T. Kiefhaber, A. Bachmann, K. S. Jensen, *Curr. Opin. Struct. Biol.* **2012**, *22*, 21–29.
- [34] E. Kim, S. Lee, A. Jeon, J. M. Choi, H.-S. Lee, S. Hohng, H.-S. Kim, *Nat. Chem. Biol.* **2013**, *9*, 313.
- [35] J. D. Johnson, M. A. El-Bayoumi, L. D. Weber, A. Tulinsky, *Biochemistry* **1979**, *18*, 1292–1296.
- [36] P. Atkins, J. de Paula, in *Atkins' Physical Chemistry 2002*, Oxford University Press, New York, **2002**, pp. 883–884.
- [37] D. D. Boehr, R. Nussinov, P. E. Wright, *Nat. Chem. Biol.* **2009**, *5*, 789–796.
- [38] H. R. Bosshard, *News Physiol. Sci.* **2001**, *16*, 171–173.
- [39] M. Andujar-Sánchez, V. Jara-Perez, E. S. Cobos, A. Cámara-Artigas, *J. Mol. Recognit.* **2011**, *24*, 548–556.
- [40] M. Novo, D. Granadero, J. Bordello, W. Al-Soufi, *J. Inclusion Phenom. Macrocyclic Chem.* **2011**, *70*, 259–268.
- [41] K. D. Danov, D. S. Valkovska, P. A. Kralchevsky, *J. Colloid Interface Sci.* **2002**, *251*, 18–25.
- [42] G. G. Hammes, Y.-C. Chang, T. G. Oas, *Proc. Natl. Acad. Sci. USA* **2009**, *106*, 13737–13741.
- [43] K. G. Daniels, N. K. Tonthat, D. R. McClure, Y.-C. Chang, X. Liu, M. A. Schumacher, C. A. Fierke, S. C. Schmidler, T. G. Oas, *J. Am. Chem. Soc.* **2014**, *136*, 822–825.
- [44] N. Greives, H.-X. Zhou, *Proc. Natl. Acad. Sci. USA* **2014**, *111*, 10197–10202.
- [45] E. N. Vasina, P. Déjardin, *Langmuir* **2004**, *20*, 8699–8706.
- [46] A. Qadeer, G. Rabbani, N. Zaidi, E. Ahmad, J. M. Khan, R. H. Khan, *PLoS ONE* **2012**, *7*, e50633.
- [47] S. Sengupta, K. K. Dey, H. S. Muddana, T. Tabouillot, M. E. Ibele, P. J. Butler, A. Sen, *J. Am. Chem. Soc.* **2013**, *135*, 1406–1414.

Received: May 5, 2015

Published online on September 14, 2015